Transformation of Furfural-Acetone Condensation Adduct over Mo/SBA-15 Catalysts under Atmospheric Pressure

Camila Abreu Teles, Carmen Ciotonea, Sebastien Royer, Frédéric Richard

catalysts

MDPI

Article

Transformation of Furfural-Acetone Condensation Adduct over Mo/SBA-15 Catalysts under Atmospheric Pressure

Camila A. Teles [1,*], Carmen Ciotonea [2], Sébastien Royer [3,4] and Frédéric Richard [1,*]

[1] Institut de Chimie des Milieux et Matériaux de Poitiers, Centre Nationale de la Recherche Scientifique-CNRS, Université de Poitiers, UMR 7285, 86022 Poitiers, France
[2] Unité de Chimie Environnementale et Interactions sur le Vivant-UCEIV, Université du Littoral Côte d'Opale, UR4492, 59375 Dunkerque, France; carmen.ciotonea@eilco.univ-littoral.fr
[3] Centrale Lille, Ecole Nationale Supérieure de Chime-ENSCL, Centre Nationale de la Recherche Scientifique-CNRS, Université de Lille, UMR 8181, 59000 Lille, France; sebastien.royer@univ-lille.fr
[4] Unité de Catalyse et de Chimie du Solide, Université Artois, UMR 8181, 59000 Lille, France
* Correspondence: camila.abreu.teles@univ-poitiers.fr (C.A.T.); frederic.richard@univ-poitiers.fr (F.R.)

Abstract: The transformation of the furfural-acetone condensation adduct (FAc) was investigated under atmospheric pressure at 300 °C over a series of molybdenum supported on SBA-15 doped with different acid/oxophilic species (Zr, Fe and Al). The FAc underwent several reactions including mainly hydrogenation, deoxygenation and cyclization. The order of activity was Mo/Zr-SBA > Mo/Al-SBA > Mo/Fe-SBA ≅ Mo/SBA, demonstrating the positive effect of dopants. Likewise, the synergy between molybdenum with the oxophilic Zr^{4+} species significantly increased the selectivity toward the partially deoxygenated products.

Keywords: biomass; jet fuel; HDO; furans; molybdenum; SBA-15

Citation: Teles, C.A.; Ciotonea, C.; Royer, S.; Richard, F. Transformation of Furfural-Acetone Condensation Adduct over Mo/SBA-15 Catalysts under Atmospheric Pressure. *Catalysts* **2023**, *13*, 1276. https://doi.org/10.3390/catal13091276

Academic Editors: Junjian Xie and Qiang Deng

Received: 26 July 2023
Revised: 31 August 2023
Accepted: 3 September 2023
Published: 5 September 2023

1. Introduction

Due to growing concerns about global climate change resulting from the use of fossil-derived energy, lignocellulosic biomass has attracted a lot of interest as a renewable resource to produce liquid fuels [1] and green valuable chemicals [2]. Contrary to gasoline and diesel engines which can be replaced in part by electric vehicles in the coming years, this cannot be the case for aircrafts. Sustainable Aviation Fuel (SAF), which can be produced from a variety of sustainable resources including biomass, is an alternative to fossil jet fuel [3]. By using SAF, the aviation industry's net-zero carbon emissions target can be reached in 2050.

The production of jet fuel range alkanes (typically C_8–C_{16} hydrocarbons) from lignocellulose derived from platform chemicals is attracting strong interest [1,4,5]. The cellulose and hemicellulose fractions of the lignocellulosic biomass can be converted into glucose and xylose, which can readily be dehydrated to produce important platform chemicals such as 5-hydroxymethylfurfural (HMF) and furfural, respectively. These compounds are good starting materials for the production of SAF. The Dumesic group [6,7] and Huber et al. [8] first reported the production of long carbon chain intermediates of C_8–C_{13} by the aldol condensation of furfural with acetone. The aldol condensation is generally performed at low temperatures (25–70 °C) under atmospheric pressure in the presence of solid basic catalysts such as NaOH, MgO-La_2O_3 and MgO-Al_2O_3 mixed oxides, and $MgF_{2-x}(OH)_x$ hydroxide fluorides, yielding mostly 4-(2-furyl)-3-buten-2-one (FAc) and 1,5-difuryl-1,4-pentadien-3-one (F_2Ac), containing eight and 13 carbon atoms, respectively [9–12].

These oxygenates can be further converted into alkanes by hydrogenation and hydrodeoxygenation (HDO) reactions in the presence of a metal-supported catalyst [13–15]. Despite a large number of works investigate the hydrogenation of furanyl compounds, a limited number is devoted to the HDO of those condensation adducts. In this case, the HDO of those compounds into n-alkanes by using metallic supported catalysts is a complex

process, including several steps to remove the oxygen atoms present in several oxygenated functions. For example, Faba et al. [13] investigated the effect of different metals (Ru, Rh, Pt and Pd) supported on alumina in the HDO of the FAc in a batch reactor operating at 120–220 °C under 5.5 MPa as H_2 pressure. The Rh and Ru-supported catalysts were only active for the hydrogenation of the aliphatic C=C bond, while the full deoxygenated product (n-octane) was obtained with selectivity around 30% for the Pd and Pt-based catalysts. The role of support (Al_2O_3, ZSM-5, L and Y zeolites, activated carbon) on the HDO of this adduct was also investigated over the Pt-supported catalysts [14]. It was highlighted that the selectivity into n-octane was improved by increasing metal dispersion, according to the results reported by Ramos et al. [15]. On the other hand, it seems that the acidic properties of the catalytic support were not beneficial for the catalytic properties of such metallic-based catalysts. The catalytic properties of several Pt-supported catalysts using different supports (SiO_2, Al_2O_3, hydrotalcite, TiO_2, beta zeolite, Al-SBA-15 and WO_3-ZrO_2) in the HDO of the FAc were also investigated at 200 °C under 5 MPa [15]. The extent of C=C and C=O hydrogenation was limited over the catalysts supported on SiO_2, hydrotalcite and Al_2O_3 but improved by the better Pt dispersion of Pt/Al-SBA-15, Pt/WO_3-ZrO_2 and Pt/HBeta. In this work, an increase of the dehydration and ring opening reactions steps with an increase in catalyst acidity was observed, thus improving the selectivity to linear alcohols. A bifunctional Pd/$NbOPO_4$ catalyst also exhibited good activity in the transformation of the FAc [16]. The metal was reported to be the active center for hydrogenation whereas the NbO_x species promoted the C-O bond cleavage of the furanic ring as well as favored dehydration steps.

Despite most of these works being conducted at the liquid phase, few works have reported the transformation of the FAc in a fixed bed reactor, operating under the gas phase. This is the case of the investigation conducted by Yang et al. [17] in which for the first time, Pd/SiO_2 and Pd-FeO_x/SiO_2 catalysts were tested in the transformation of the aldol condensation adduct of furfural and methyl-isobutylketone (MIBK) without a solvent at 350 °C under atmospheric pressure. While a 5%Pd/SiO_2 catalyst yielded about 60% of 2-methyldecane and 2-methylnonane as deoxygenated compounds, the catalyst promoted with iron (5%Pd − 2.5%FeO_x/SiO_2) produced up to 90% of these compounds. The promoter effect of iron was attributed to both the generation of the Pd-Fe alloy and the partially reduced FeOx species that allowed the deoxygenation of the furan compound.

The development of such a process under the gas phase is highly desired due to several advantages, such as easy scalability at the industrial level, easy separation and regeneration of the catalyst, and carbon coverage can be mitigated in a flow fixed-bed reaction by controlling the operating parameters [18]. Besides that, operating at atmospheric pressure, the consumption of hydrogen is limited, ideal for the production of SAF. Therefore, in the present work, we investigated the transformation of the FAc under atmospheric pressure in a fixed-bed flow reactor operating at 300 °C. Owing to its high surface area and ordered mesopores distribution, the SBA-15 type silica was used to disperse the MoO_x species, known to be active in the cleavage of the C-O bond [19,20]. To explore the effect of adding oxophilic or acidic sites, SBA-15 was also doped with a low content of different species (Zr, Fe and Al). To the best of our knowledge, it was the first time that the catalytic properties of such solids were investigated for the transformation of the aldol condensation adduct over molybdenum-based catalysts. Hence, new products were identified, and different reaction pathways were proposed to explain the reactivity of the FAc.

2. Results and Discussion

2.1. Catalyst Synthesis and Characterization

A set of molybdenum supported on silica type SBA-15 and functionalized SBA-15 with different species (Zr, Fe and Al) has been prepared. The functionalized supports were prepared through different methods proposed in the literature in order to achieve a good homogeneity and dispersion of the dopants into the support [21,22]. In the case of Fe-SBA and Zr-SBA, simpler and effective methods were used: melting infiltration and incipient

wetness impregnation, respectively [21]. A pH-adjusting method was used to prepare the Al-SBA material, in an attempt to incorporate aluminium atoms in the silica framework while maintaining the ordered meso-structure [22].

The elementary analysis showed that the Mo content was close to the expected value (35 wt.%) and the content of the support dopant was between 2.4 and 2.7 wt.% in the final catalyst (Table 1). The textural properties of the catalysts and the respective bare supports were investigated by N_2 physisorption (Figure 1). All the materials presented a N_2 adsorption/desorption isotherm type IV with H1 hysteresis which is characteristic of ordered mesoporous materials with a narrow distribution of cylindrical channels, an arrangement typical of SBA-15. The same profile was observed for the functionalized supports, presenting isotherms with steeper adsorption/desorption branches and the well-defined hysteresis, reflecting a higher degree of pore size uniformity. This indicates that the methodologies used to functionalize the SBA-15 did not modify the pore structure of SBA-15. After introducing molybdenum, the isotherms presented less regular hysteresis loops, which indicate a broader pore size distribution [23].

Table 1. Elemental composition and textural properties of the materials.

Sample	wt. (%)				SSA ($m^2\ g^{-1}$)	S_{micro} ($m^2\ g^{-1}$)	V_p ($m^3\ g^{-1}$)	V_{micro} ($m^3\ g^{-1}$)	D_p (nm)
	Mo	Zr	Fe	Al					
SBA-15	-	-	-	-	817	225	1.23	0.019	9.0
Mo/SBA	33.7	-	-	-	213	18	0.42	0.007	7.7
Zr-SBA	-	3.8	-	-	621	101	0.88	0.044	6.4
Mo/Zr-SBA	36.3	2.4	-	-	195	36	0.34	0.017	6.4
Fe-SBA	-	-	4.2	-	721	157	0.97	0.068	6.6
Mo/Fe-SBA	36.1	-	2.7	-	132	24	0.27	0.011	7.0
Al-SBA	-	-	-	4.1	339	51	0.83	0.021	8.2
Mo/Al-SBA	34.0	-	-	2.7	86	25	0.20	0.012	7.5

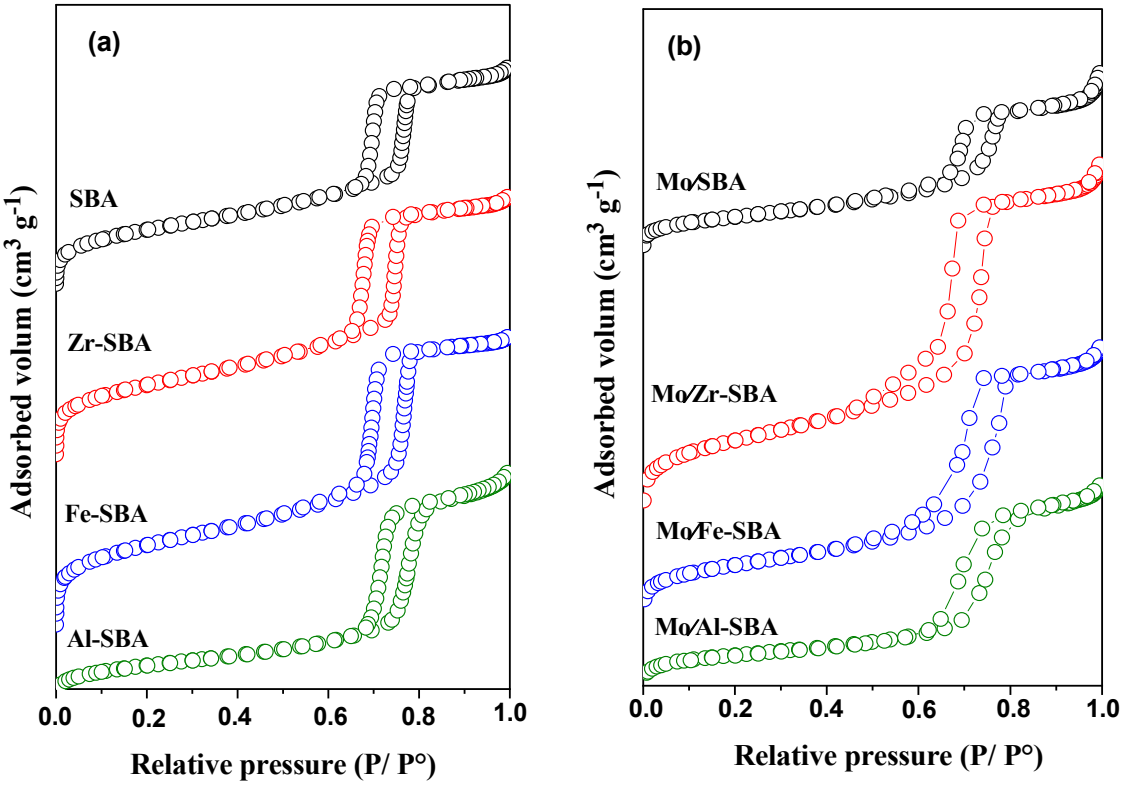

Figure 1. (**a**) N_2 adsorption−desorption isotherms for the supports and (**b**) the respectively supported catalysts.

The pore size distribution curves for the bare supports and for the supported molybdenum catalysts are presented on Figure 2. A narrow pore size distribution can be observed for the functionalized supports, in accordance with defined hysteresis observed. After the introduction of molybdenum, the correspondent curves show a broader pore size distribution, especially for the Mo/Fe-SBA and Mo/Al-SBA catalysts, which is related to the partial filling of the pores by the molybdenum oxide phase, thus creating a new porosity.

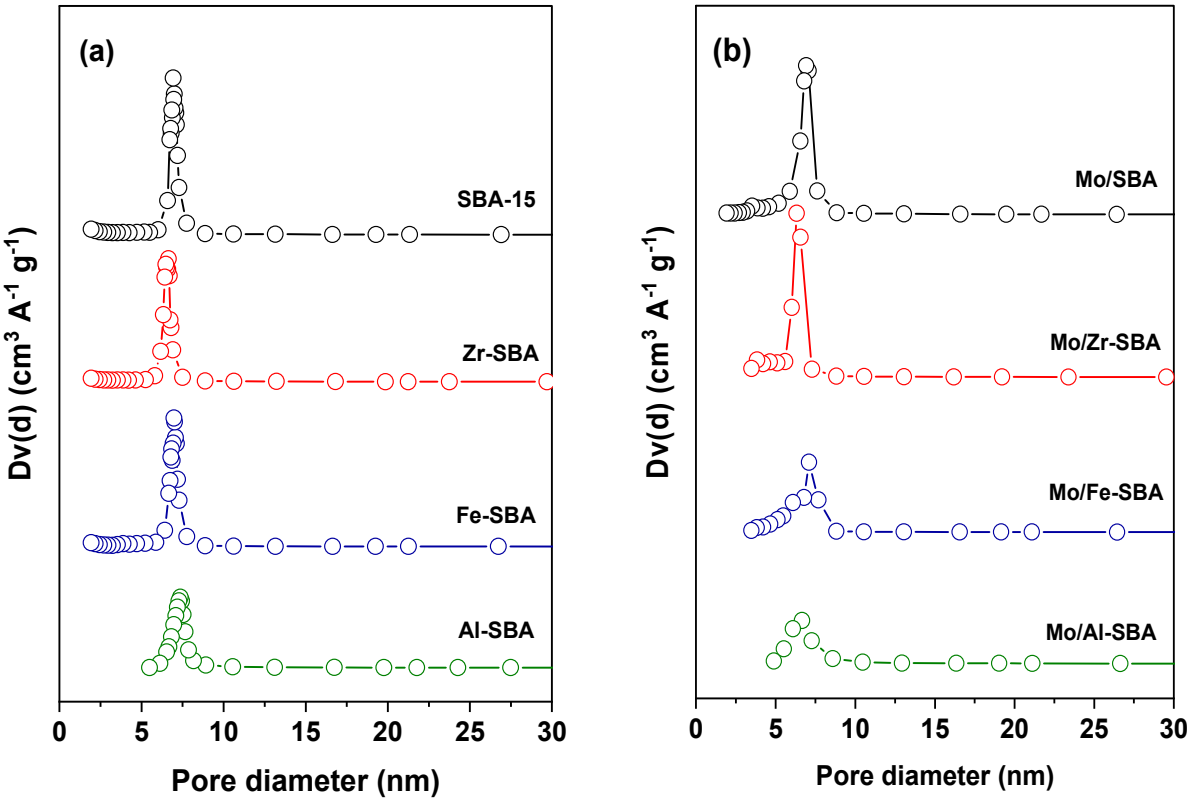

Figure 2. Pore size distribution for the (**a**) bare supports and (**b**) supported molybdenum catalysts obtained from N_2 adsorption−desorption experiments using the BJH method.

As indicated in Table 1, the surface area of the supported catalysts significantly decreased compared to the respective bare supports, which was accompanied by a decrease of the pore volume; such a decrease was higher than usually reported in the literature for MoO_3-supported catalysts [20,24,25]. This drastic decrease of the textural properties can be explained in part by the high quantity of Mo deposited leading to a partial filling of the pores by the molybdenum oxide phase, and thus, the consequent partial blockage of the mesopores as well as the micropores. Herein, the accessible surface area of the catalysts varied between 86 to 213 $m^2\ g^{-1}$ depending on the sample.

The low angle XRD patterns of the bare supports and the following introduction of molybdenum, as well as high-angle XRD patterns of the catalysts, are shown in Figure 3. The ordering porosity of the different functionalized supports was confirmed by the presence of the three main diffractions peaks associated with the planes (100), (110) and (200), characteristic of the ordered hexagonal pore arrangement in the mesoporous network of SBA-15. This indicates that the introduction of the dopants did not modify the ordering typically found for the SBA-15-like 2D pore network. After the introduction of molybdenum, those three peaks were always observed, indicating that the mesopore structure was preserved. In addition, a broadening of the main reflection and a slight shift to higher 2θ values compared to the respective supports were observed. This might be caused by a possible slight distortion of the mesoporous channels due to the deposition of MoO_3 clusters on the pore walls. Regarding the XRD patterns of the supported catalysts, intense

reflections characteristic of the MoO_3 phase (PDF 05-0508) were observed. The high intensity of those reflections indicates the formation of large crystallites poorly dispersed on the supports, probably located at the external surface of SBA-15, after pore filling.

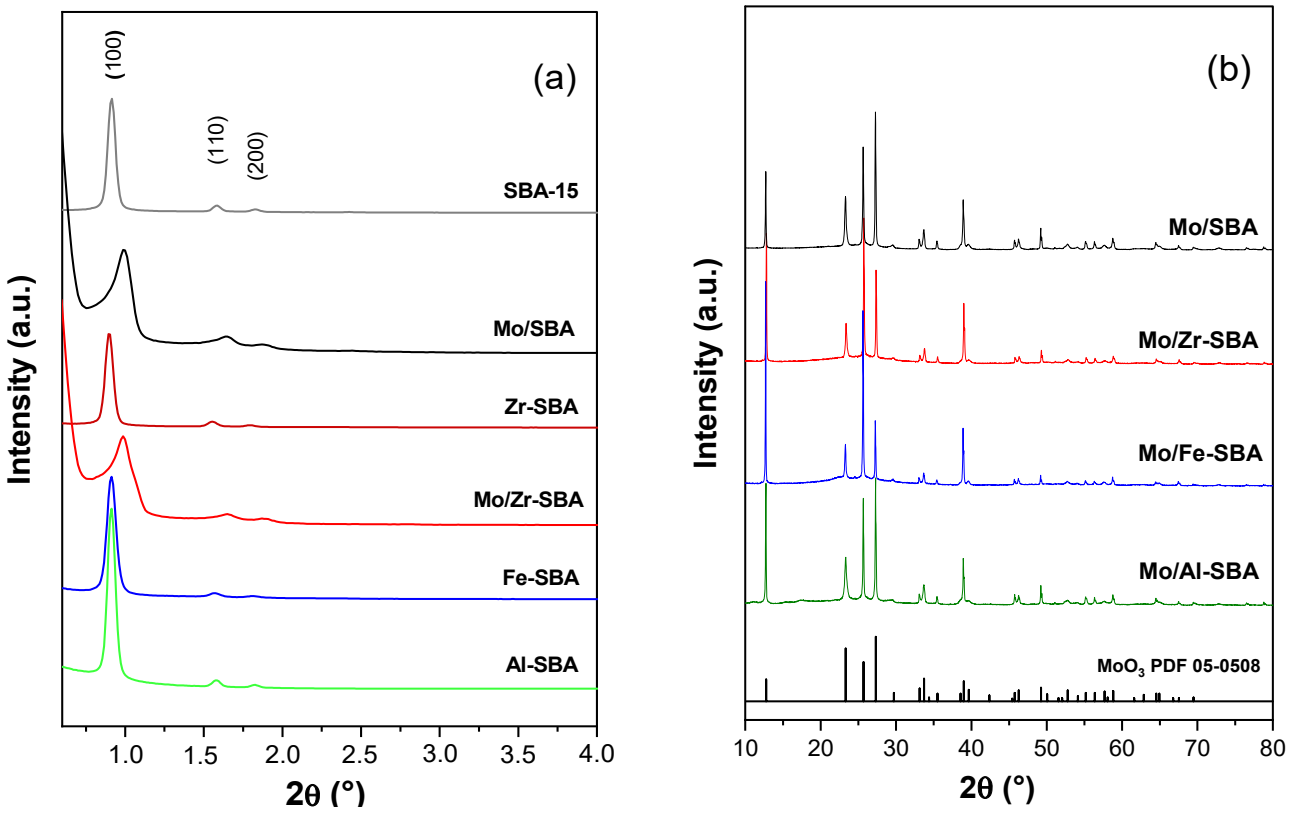

Figure 3. (**a**) Low angle XRD patterns of the supports and (**b**) high angle XRD patterns of the supported catalysts; bottom, the ICDD reference.

The reducibility of molybdenum oxide was evaluated by the H_2-TPR analysis (Figure 4). In general, molybdenum oxide reduces in two steps: (i) Mo(VI) to Mo(IV) in a temperature range of 450–650 °C, and (ii) Mo(IV) to Mo(0) at temperatures up to 700 °C [26,27]. In our work, these two main reduction events are observed: the first one in the region between 450 to 650 °C and the second one between 650 to 950 °C. However, in our case, the first event is split into two peaks (centered at around 560 ad 610 °C). This may be due to the reduction of the MoO_3 species present inside and outside the porosity of SBA-15. All the supported catalysts presented a similar reduction profile. However, the peaks are slightly shifted to higher temperatures in the Mo/Fe-SBA and Mo/Al-SBA samples, suggesting a stronger interaction between the MoO_3 species and the dopants. For all the samples, MoO_3 was completely reduced in the temperature range analyzed (Table 2).

The acidic properties of the catalysts were investigated by pyridine adsorption–desorption DRIFTS experiments. The total acidity of each solid as well as their acid site distribution are presented in Table 2. As expected, no bands were observed in the bare SBA-15 support, indicating the absence of noticeable acidity for this support. The presence of MoO_3 species led to the appearance of bands associated with pyridine adsorbed on the Lewis acid sites (located at 1456 cm^{-1} and 1624 cm^{-1}); pyridine adsorbed on the Brønsted acid sites (band located at 1547 cm^{-1}) and with both acid sites at around 1490 cm^{-1} [28]. The Mo/SBA catalyst exhibited a density of acid sites of 93 μmol g^{-1} being mainly of Lewis type, attributed to the presence of the molybdenum oxide phase. The introduction of a small content of dopant onto the silica support allowed the creation of acid sites (density of acid sites varying between 98 to 171 μmol g^{-1} depending on the dopant). With the introduction of the MoO_3 species, the density of the acid sites decreased, which is probably due to

the partial blockage of the pores, as observed from the N_2 adsorption desorption results (Table 1). Indeed, the presence of the oxide phase seems to decrease the accessibility of the acid sites inside the SBA-15 channels. Comparing the catalysts containing the dopant in the structure of SBA-15, the density of the Brønsted acid sites remained almost constant (27–31 µmol g^{-1}), while the Lewis acid sites varied depending on the nature of the dopant (Zr-SBA > Al-SBA > Fe-SBA).

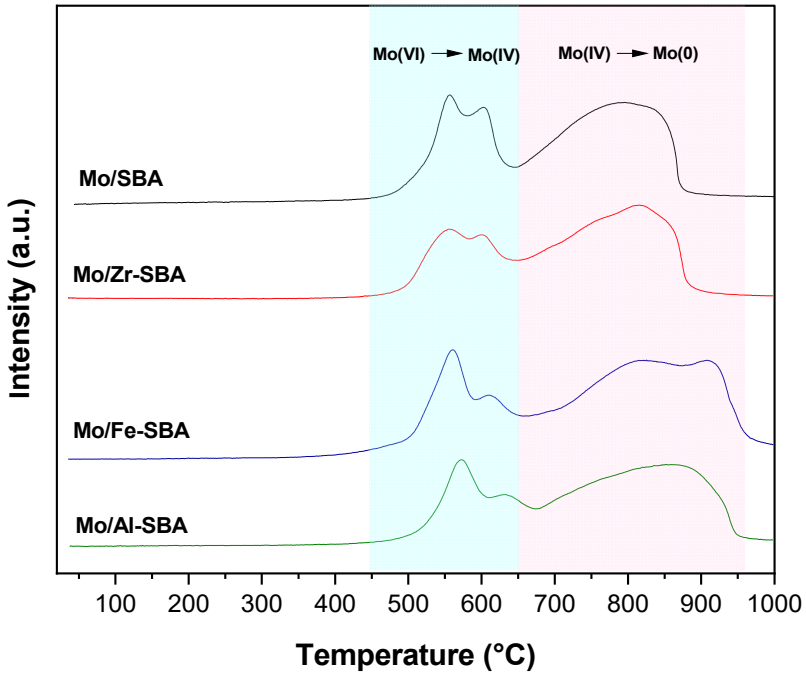

Figure 4. H_2-TPR profile of the molybdenum-based catalysts.

Table 2. Redox and acid properties of the materials.

Sample	H_2 Uptake (mmol g^{-1})		O_2 Uptake [c] (µmol g^{-1})	Redox Mo [d] (%)	Total Acidity [e] (µmol g^{-1})	Acid Sites Distribution [e] (µmol g^{-1})	
	Exp. [a]	Cal. [b]				Brønsted	Lewis
Mo/SBA	10.5	10.4	56	2.8	93 (0)	10 (0)	83 (0)
Mo/Zr-SBA	11.2	11.3	131	6.9	120 (106)	31 (8)	89 (98)
Mo/Fe-SBA	11.9	11.3	56	2.8	90 (98)	27 (14)	63 (84)
Mo/Al-SBA	11.4	10.6	51	3.0	100 (171)	30 (37)	70 (134)

[a] Quantity of H_2 determined from TPR experiments; [b] Quantity of H_2 calculated according to the theoretical reduction of Mo(VI) into Mo(0); [c] O_2 uptake measured by chemisorption of O_2; [d] Calculated from the equation: % Redox Mo = (2 × oxygen uptake/Mo loading) × 100; [e] Quantity of pyridine adsorbed in µmol g^{-1}. The values in brackets represent the values obtained for the respective bare supports.

The oxygen uptake measurement was used to estimate the number of active Mo species (Table 2). Indeed, Shetty et al. demonstrated that the oxygen chemisorption is an efficient technique to determine the number of oxygen vacancies present in molybdenum oxide supported catalysts which are considered as an active phase for the HDO of phenolic molecules [20]. For the Mo/SBA sample, the O_2 uptake value was 56 µmol g^{-1}, significantly lower compared to the one obtained by Gonçalves et al. for a 10wt.%Mo/SBA sample (163 µmol g^{-1}) [20]. This may be due to the larger MoO_3 crystallites obtained here, thus presenting a lower exposed surface to chemisorb oxygen. These crystallites may also block the pores mouth, hampering the adsorption of oxygen with the molybdenum species confined in the support mesoporosity. Comparing the different samples, the values of O_2 uptake were similar for the Mo/SBA, Mo/Fe-SBA and Mo/Al-SBA samples while 2.3 fold

higher for Mo/Zr-SBA (131 μmol g^{-1}), thus the latter presented a number two times higher than that of the redox Mo sites.

2.2. Catalytic Transformation of 4-(2-furyl)-3-buten-2-one

A series of preliminary tests was performed in order to establish the most appropriate reaction conditions to conduct the catalytic experiments. Due to the very low miscibility of the reactant in nonpolar solvents, ethanol was used as a solvent, this being already used in previous works. It is known that light alcohols may act as a hydrogen donor and thus, in the presence of specific catalysts, it could promote a catalytic transfer hydrogenation (CTH) reaction [29]. However, in our case, the reaction was carried out under the flow of molecular hydrogen, thus minimizing the contribution of CTH. Besides that, it is well established that secondary alcohols are more effective for CTH than primary alcohols such as ethanol [29]. The reaction conditions (300 °C and atmospheric pressure) were chosen based on the previous work conducted by our group for the HDO of phenolic compounds [28,30], as well as reported in the literature for the deoxygenation of furfural [31,32].

The conversion and product distribution obtained after 30 min on the stream are presented in Table 3. The supports without molybdenum did not show measurable conversion in such reaction conditions, indicating that bare supports were inactive. Mo/SBA and Mo/Fe-SBA showed a similar conversion at the same contact time (W/F = 73 mmol g^{-1} h^{-1}), which is defined as the ratio of the catalyst weight (in g) and the molar flow of the reactant (in mol h^{-1}), with Mo/Zr-SBA and Mo/Al-SBA presenting a 41 and 32% conversion, respectively. The order of activity, determined by the calculated reaction rates was Mo/Zr-SBA (5.6 mmol g^{-1} h^{-1}) > Mo/Al-SBA (4.4 mmol g^{-1} h^{-1}) > Mo/Fe-SBA (2.1 mmol g^{-1} h^{-1}) ≅ Mo/SBA (2.0 mmol g^{-1} h^{-1}).

Table 3. Product distribution for the transformation of 4-(2-furyl)-3-buten-2-one (FAc) over the catalysts at a same W/F equal to 73 g h mol^{-1} (T = 300 °C, atmospheric pressure, 30 min of Time on Stream).

Sample	X [a] (%)	Selectivity (mol %) [b]							
		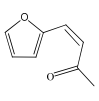	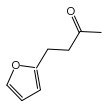	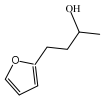	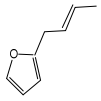	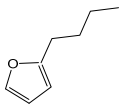	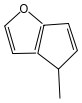	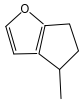	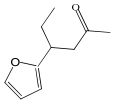
		A	B	C	D	E	F	G	H
Mo/SBA	15	16	17	-	-	-	27	12	28
Mo/Zr-SBA	41	4	11	1	-	-	63	10	11
Mo/Fe-SBA	15	16	19	-	-	-	26	10	29
Mo/Al-SBA	32	7	32	-	1	1	30	15	14

[a]: the total conversion of the FAc was calculated using Equation (1) given in the experimental part. [b]: the percentage molar of each product obtained was calculated using Equation (2) given in the experimental part.

Due to the complexity of the products' nomenclature, each compound was labeled with a capital letter to be used during the discussion. The conversion of the FAc usually involves different reaction steps, mainly including hydrogenation, dehydration and ring-opening reactions. Furthermore, some additional side reactions such as isomerization, cyclization or condensation occur depending on the catalysts' properties such as acidity, resulting in a diverse product distribution. The reaction pathways proposed in our work are showed in Scheme 1. Herein, for all catalysts, the major product obtained was 4-(2-furyl)-butan-2-one (B), related to the selective hydrogenation of the aliphatic C=C bond, being mainly produced over the Mo/Al-SBA catalyst (32% of selectivity). This is in accordance with works performed in the liquid phase, suggesting that the hydrogenation of the conjugated C=C bond is favored compared to the direct hydrogenation of the C=O bond. The alcohol C, obtained from hydrogenation of the C=O bond of B, was only detected in traces from all catalysts used. This result can be explained by its high reactivity leading to F through the dehydration or hydrogenolysis of the C–O bond followed by cyclization, with further

partial ring hydrogenation to give G. To the best of our knowledge, the formation of both products from the FAc were never reported in the literature, probably because such molybdenum-based catalysts were never used for such a reaction. Thus, these compounds were obtained as main products in our work, being mostly formed over the Mo/Zr-SBA catalyst (73 mol% compared to around 40 mol% for the other catalysts).

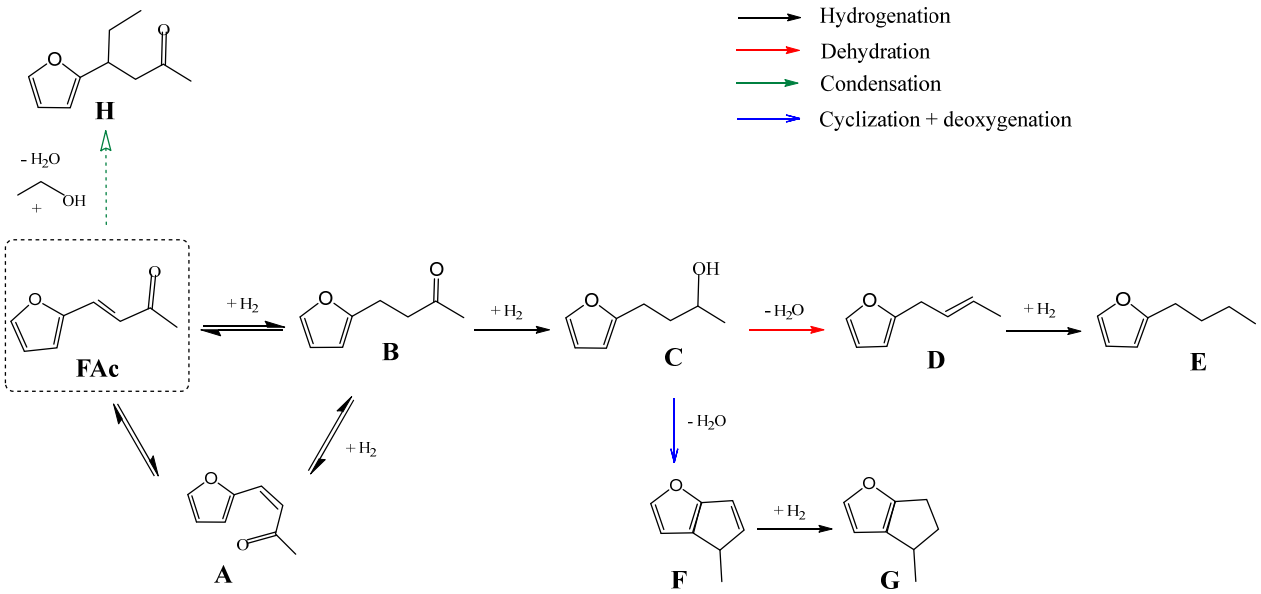

Scheme 1. Proposed reaction scheme for the transformation of 4-(2-furyl)-3-buten-2-one at the gas phase, atmospheric pressure and reaction temperature of 300 °C over the molybdenum−based catalysts.

Besides those products, A and H were also formed to a considerable extent as a result of the isomerization of our reactant (FAc) and by condensation with ethanol used as a solvent, respectively. Both compounds were mainly produced over the Mo/SBA and Mo/Fe-SBA catalysts which exhibited the lowest acidity (Table 2). However, linear carbon chain products were never observed in our work, probably due to the low pressure used. Thus, all products obtained were not fully deoxygenated and cannot be blended directly in SAF; this feedstock mainly contains deoxygenated products. In order to favor the full deoxygenation of the FAc, more severe experimental conditions (pressure and/or temperature) have to be used. It is well known that the heat of combustion (energy content) of oxygenated molecules is lower compared to the corresponding deoxygenated molecules and thus, the energy content of the main product obtained here is still lower compared to SAF. For example, the calorific value of furan-based compounds such as dimethylfuran is 33.7 MJ/kg compared to 43 MJ/kg of SAF. As a consequence, the energy content of the mixture obtained under our experimental conditions is probably lower than the one of SAF.

Regarding the literature about the transformation of the FAc, most of the works are performed at the liquid phase using a higher H_2 pressure and mainly noble metal-supported catalysts. The reaction pressure has an important role and may determine the product distribution. A higher H_2 pressure facilitates the hydrogenation steps and ring-opening, thus resulting in linear alcohols which in turn, can be converted to linear alkanes via the dehydration reaction, promoted by acid sites. For example, Faba et al. investigated the effect of different metals (Pt, Pd, Rh and Ru) supported on alumina, as well as Pt loaded on different supports (ZSM-5, L and Y zeolites and high surface area graphite and activated carbon) in the transformation of the FAc at the liquid phase under 2.5 MPa of H_2 [13,14]. Concerning the type of metal, Rh and Ru supported on alumina were only active for the hydrogenation of the aliphatic double bond, thus yielding the product B. Instead, Pd and, especially, Pt-based catalysts, were active for the total deoxygenation of the condensation adduct, producing n-octane as a final product. The different behavior of the catalysts was attributed to the different affinity between the metal crystallites with the reactant

and reaction intermediates. By testing Pt loaded on the different supports, the authors demonstrated that the first reaction step (hydrogenation of the aliphatic C=C bond) is structure-sensitive, mostly depending on the metal dispersion. Moreover, further steps involving the ring opening and deoxygenation depend on the acid-base properties of the support; the acidity of the support has not only any positive effect on the deoxygenation, but also favors the formation of unreactive intermediates that remain adsorbed on the catalyst surface causing deactivation. Pt supported on others supports (SiO_2, Al_2O_3, TiO_2, Beta zeolite, Al-SBA-15 and WO_3-ZrO_2) were investigated by Ramos et al. in the liquid phase at 200 °C and 5 MPa of H_2 [15]. All of the catalysts showed good activity for the hydrogenation of the aliphatic C=C bond, producing A as the main product. Further hydrogenation of the carbonyl group to produce C and E was promoted by the catalysts containing acid sites. In that work, the selectivity to linear alcohols was very low, limited by the slow rate of dehydration and ring-opening steps, and alkanes was never observed, as in our case. Besides that, over Pt supported on Al-SBA-15 and WO_3-ZrO_2, a side aldol condensation reaction took place between carbonyl containing intermediates and acetone, yielding longer carbon chain compounds.

Performing this reaction under gas phase is highly desired due to the advantages such as easy scalability and efficiency in an industrial application. However, very few have been interested in this until now. For instance, Yang et al. investigated the HDO of the aldol condensation product of furfural and methyl-isobutylketone (MIBK) using a fixed-bed reactor and without using a solvent, at 350 °C and varying hydrogen pressures between 1 to 60 bar; thus, the reaction was performed at atmospheric pressure for the first time [17]. In that work, Pd/SiO_2 and Pd-FeO_x/SiO_2 catalysts were evaluated. Jet fuel range alkanes, mainly composed of 2-methyl-decane and 2-methyl-nonane, were obtained over both catalysts under high pressure conditions, and the carbon yield was greatly improved over the iron promoted catalyst. When tested under atmospheric pressure conditions, such a catalyst (Pd-FeO_x/SiO_2) adduct was completely converted at 350 °C, achieving 64% of selectivity to those alkanes. The superior HDO activity of the Pd-FeO_x/SiO_2 catalyst was attributed to the formation of the Pd-Fe alloy and partially reduced FeO_x species which promotes hydrogenolysis and the hydrogenation of the carbonyl group over Pd, restraining decarbonylation and thus avoiding the formation of shorter chain alkanes.

In the present work, operating at 300 °C under atmospheric pressure, over molybdenum-based catalysts restricted hydrogenation of the furan ring. Indeed, the carbonyl group was first hydrogenated to produce an alcohol (C) which in turn may be dehydrated to produce (D) over acid sites, or through hydrogenolysis of the C-OH bond to eliminate the oxygen followed by cyclization, resulting in the major product (F).

No correlation can be deduced between the catalyst activity or its selectivity to partial deoxygenated products with catalyst acidity. Indeed, Mo/Zr-SBA is active by an amount 2-fold higher than the Mo/SBA and Mo/Fe-SBA catalysts, while its acid sites density is slightly higher. Also, Mo/Zr-SBA presented a higher content of oxygen vacancies, as determined by O_2 uptake (Table 2), thus in agreement with the superior activity of this catalyst. This might suggest that the nature of the dopant plays a key role in the activation of reaction intermediates and thus, the synergy between Mo and Zr is responsible for its greater performance in the partial deoxygenation of the FAc. The literature reports the superior efficiency of molybdenum oxide in the C–O bond hydrogenolysis of biomass derived oxygenates (such as phenolics [19,20,33], ketones and cyclic ethers [34], triacylglycerides [35]. Partially reduced MoO_3 will promote the adsorption of the oxygen-containing functional group on the vacancy site following the C–O bond cleavage by hydrogenolysis, and then further regeneration of the vacancy with H_2. The synergism effect of MoO_x with oxophilic species such as Zr^{4+} can also enhance the HDO activity of Mo-based catalysts, as recently demonstrated by Farah et al. [36].

2.3. Catalyst Stability

The stability of the catalysts was investigated by following the FAc conversion during 4.5 h on stream. All of the catalysts showed a decrease in the FAc conversion with time. Considering Mo/SBA (Figure 5A) and Mo/Fe-SBA (Figure 5D), both catalysts exhibited the lowest activity, after 4.5 h on stream, the FAc conversion being close to 9% and 5%, respectively. The selectivity into A increased with time on stream (TOS) and it was the main product after 4.5 h on stream (35 mol% for Mo/SBA and 60 mol% for Mo/Fe-SBA). This product was obtained by the isomerization of the double C=C bond (trans into cis) which involved only acid sites, its formation probably being very easy to occur. This suggests that sites responsible for deoxygenation are being deactivated and the product B is no longer converted. For the more active catalysts (Mo/Zr-SBA and Mo/Al-SBA), no important differences in selectivity are observed during the reaction time. In the first case (Mo/Zr-SBA, Figure 5B), F was the main product irrespective of TOS. For Mo/Al-SBA (Figure 5C), B and F were observed in equimolar amounts.

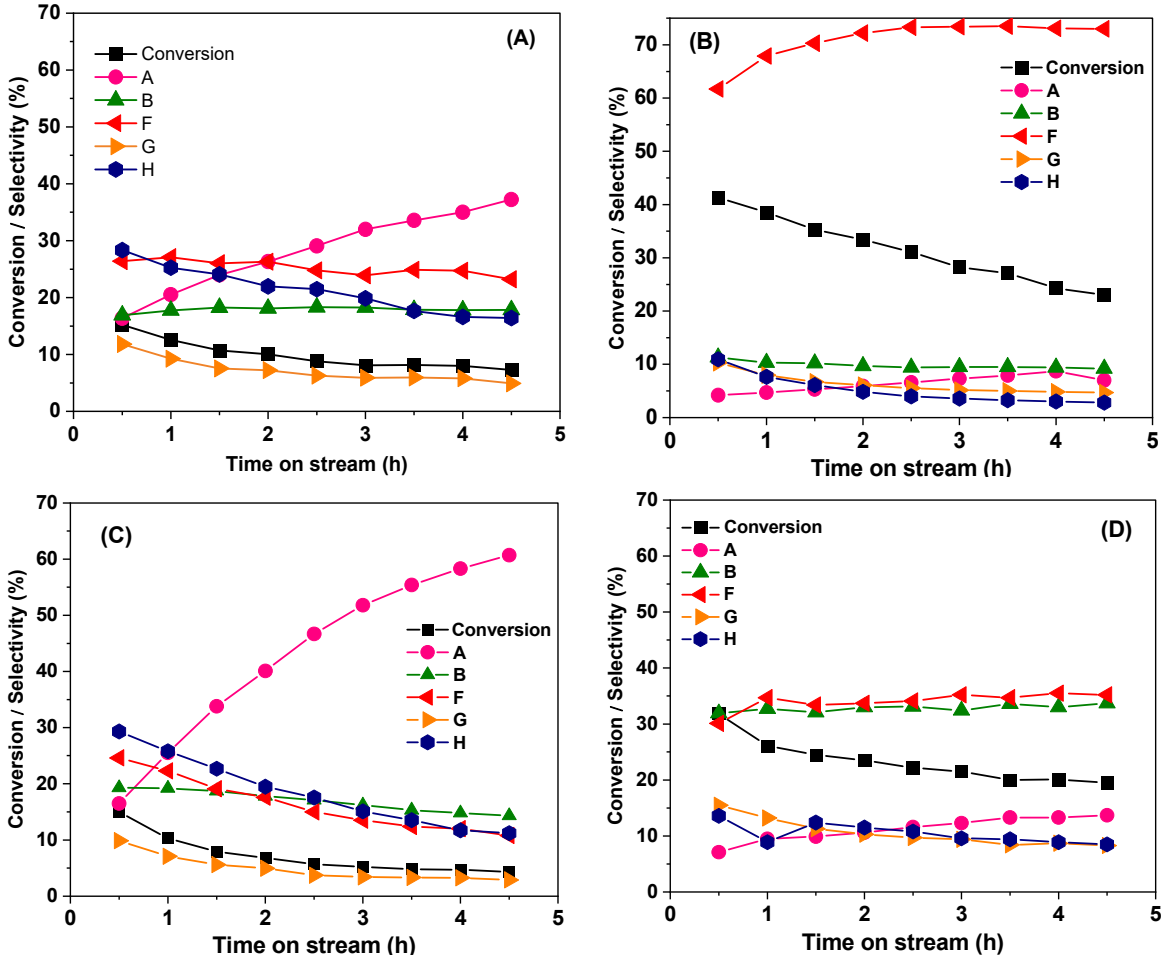

Figure 5. Conversion of 4-(2-furyl)-3-buten-2-one as a function of TOS for the molybdenum-based catalysts at 300 °C and atmospheric pressure (w/F = 73 g. h mol^{-1}). (**A**) Mo/SBA; (**B**) Mo/Zr-SBA; (**C**) Mo/Fe-SBA; and (**D**) Mo/Al-SBA.

In order to determine the presence of adsorbed organic compounds and/or coke deposits, the TG analysis coupled with a mass spectrometer was performed over the spent catalysts (Figure 6). The first weight loss observed in the TG profile (Figure 6a) in the region of 200 to 450 °C can be correlated with the CO_2 evolution showed on Figure 6b, and reveals the presence of organic compounds over the spent catalyst. The second strong weight loss starting at 700 °C is due to the thermal decomposition of MoO_3 [37]. For the Mo/SBA

catalyst, the less active catalyst, a broad peak with a low intensity compared to other catalysts was centered at 350 °C, indicating that its low activity cannot be explained by coke deposition. For Mo/Zr-SBA, the most active catalyst, two main and very intense peaks were observed at 320 and 382 °C while for Mo/Fe-SBA, a well-defined peak at 355 with a shoulder at around 280 °C can be observed. Mo/Al-SBA showed a similar profile compared to Mo/Zr-SBA but the peaks slightly shifted to higher temperatures (330 and 385 °C). Taking into account that the combustion happens at relatively low temperatures (until around 450 °C), we could suggest that the observed peaks are due to the oxidation of strongly adsorbed intermediate species on the catalytic surface. When Faba et al. performed the transformation of the FAc over a Pt/Al_2O_3 catalyst, the analysis of the spent catalyst showed an intense peak in the region of 327–627 °C. The authors attributed this peak to the oxidation of carbon deposits on the catalyst surface [13]. In our work, the Mo/Zr-SBA and Mo/Al-SBA catalysts showed a higher formation of CO_2, in agreement with the weight loss measured in the TG analysis: Mo/Zr-SBA (9.6% $g/g_{catalyst}$) = Mo/Al-SBA (9.6% $g/g_{catalyst}$) > Mo/Fe-SBA (7.5% $g/g_{catalyst}$) > Mo/SBA (5.8% $g/g_{catalyst}$). Therefore, we can suggest that the blockage of the active sites by organic adsorbed compounds could be the main cause of the catalyst deactivation.

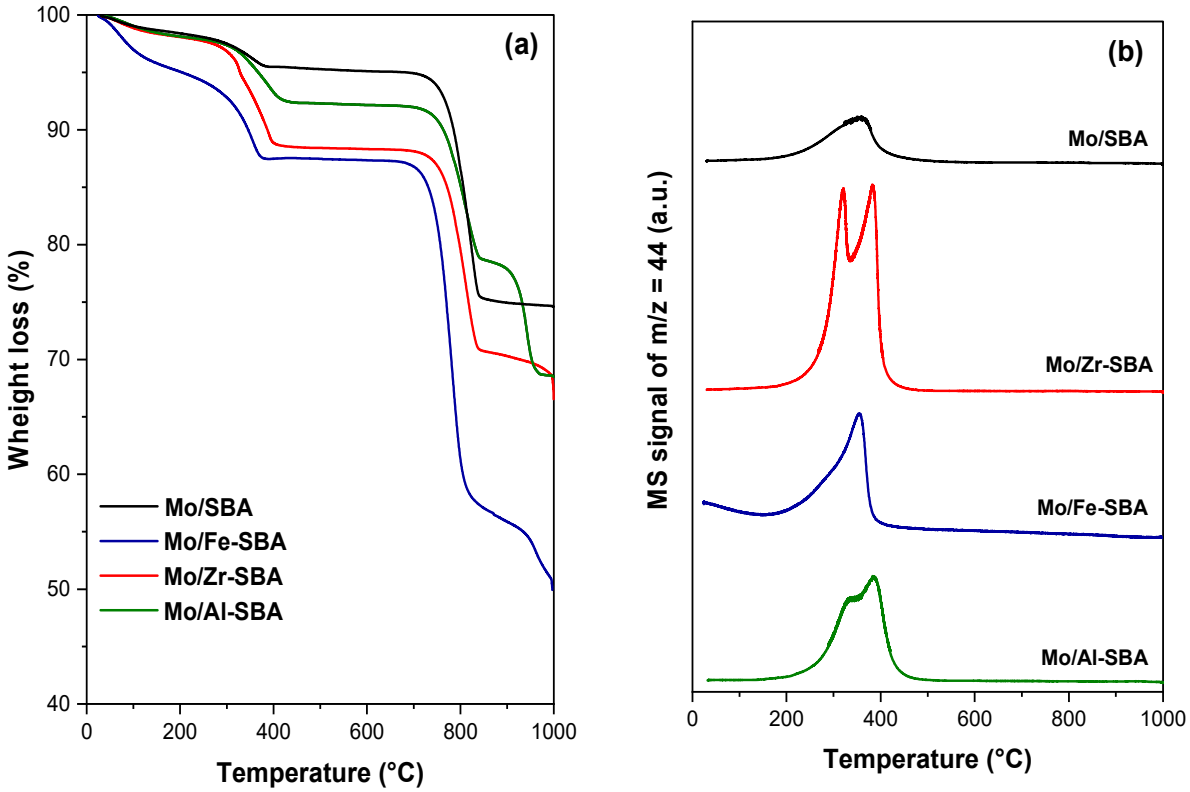

Figure 6. (**a**) TG profiles of spent catalysts after transformation of the FAc and (**b**) MS signal of CO_2 release during TG analysis.

3. Materials and Methods

3.1. Support Preparation

The ordered mesoporous SBA-15 support was prepared by a conventional templating method. An amount of 4.0 g of the structure directing agent (Pluronic P123) was solubilized in 150 mL of 1.6 M HCl at 40 °C under continuous stirring. Then, 8.5 g of TEOS, used as the silicon source, was added dropwise and the solution was thus maintained under stirring at 40 °C over 24 h. The resulting mixture was thermally treated at 100 °C during 48 h in a PTFE steel lined autoclave. The solid was then recovered by filtration and intensively washed with deionized water. The solid was dried at 100 °C for 24 h and further calcined

at 550 °C for 6 h (1.5 °C min^{-1}) to remove the organic template. The prepared support was denoted as SBA-15.

The surface chemistry of the SBA was modified by functionalization of the silica, x-SBA-15 with x = Al, Zr and Fe adapted in order to obtain a homogenous distribution of the second element, the desired content of each element (Al, Zr or Fe) being 4.0 wt%.

Al-SBA support was prepared by the two-steps pH-adjusting method [23]. The procedure is similar the one used to prepare SBA-15. However, after addition of TEOS to the acidic solution containing P123, the solution was aged for 4 h under stirring and then, the aluminum precursor ($Al(NO_3)_3 \cdot 9H_2O$) was added with the final solution being aged for more than 20 h under continuous stirring. The resulting gel was then subjected to a hydrothermal treatment at 100 °C for 48 h. After this, the resulting suspension was cooled down to an ambient temperature and the pH was adjusted to 7.5 with a 4 M ammonia solution. The suspension was then subjected to a second hydrothermal treatment at 100 °C for more 48 h. The final solid was recovered by filtration, washed and dried at 100 °C for 12 h and further calcined at the same conditions used for the SBA-15.

Zr-SBA support was prepared by incipient wetness impregnation (IWI) [20]. The aqueous solution of the Zr precursor ($ZrOCl_2.8H_2O$) was homogenized with the calcined SBA-15 and further dried at 25 °C over 5 days. The resulting solid was then calcined at 500 °C for 6 h (1.5 °C min^{-1}).

In the case of Fe-SBA support, the melt infiltration method was used, as described elsewhere [21]. For the preparation, $Fe(NO_3)_3.H_2O$ was ground with uncalcined SBA-15 until the obtention of well-homogenized powder. For the infiltration treatment, the solid was transferred to the Teflon-lined autoclave for 4 days at the melting temperature of the precursor. Further, the solid was calcined at 500 °C for 6 h (1.5 °C min^{-1}).

3.2. Catalyst Preparation

Molybdenum-supported catalysts were prepared by the incipient wetness impregnation (IWI) method. Aqueous solutions of the Mo precursor, $(NH_4)_6Mo_7O_{24}.4H_2O$, were prepared to obtain a loading degree of 35 wt.% Mo, and the volume of impregnation solutions was adjusted to the pore volume of the support. The solutions were homogenized with the supports and then, the solids were transferred to an oven at 25 °C for 5 days. The catalysts were finally calcined under air at 400 °C for 3 h (heating ramp of 2 °C min^{-1}). The materials were denoted as Mo/X-SBA (X = Zr, Fe and Al).

3.3. Catalyst Characterization

Elementary analysis of the calcined samples was performed by inductively coupled plasma optical emission spectroscopy (ICP-OES) using a SPECTRO ARCOS ICP-OES instrument. Prior to the analysis, the samples were digested with concentrated nitric and hydrofluoric acid using a microwave heating system.

Textural properties of the catalysts were obtained by N_2 physisorption at −196 °C on a Micromeritics Tristar II automated gas sorption system, operated with a software MicroActive version 4.06. Before the analysis, the samples were outgassed under a vacuum at 300 °C for 3 h. The specific surface areas were calculated using the B.E.T. method in the 0.10–0.25 p/p_0 interval. The T plot method was used for calculating the microporous volume and surface area. The mesopore size distribution was plotted by using the B.J.H. method applied to the desorption branch of the isotherms. For the calculation of Vp, p/p_0 = 0. 99 was used.

A small angle X-ray scattering (SAXS) analysis was obtained in order to investigate the order of the pore network for the supports. Experiments were performed on a Xeuss 2.0 (Xenocs) system operated under a vacuum with a GeniX3D micro-source (λ = 1.54 Å) at 0.6 mA and 50 kV, and a 2D Pilatus 3R 200K detector. The sample-to-detector distance was 1005 mm.

The determination of the crystalline phase was performed by an X-ray diffraction (XRD) analysis, using a Bruker X-ray AXS D8 Advance diffractometer in the Bragg–Brentano

geometry configuration fitted with a LynxEye Super Speed detector. The XRD patterns were recorded with Cu Kα radiation (λ = 0.154 nm, 40 kV, 30 mA) in the 10–80° 2θ range (0.02° 2θ step).

Molybdenum reducibility was determined by a temperature-programmed reduction (H_2-TPR) analysis. Experiments were conducted on an Autochem chemisorption analyzer (Micromeritics). The samples were pre-treated under 50 mL min^{-1} of synthetic air at 200 °C (10 °C min^{-1}, 1 h) and then cooled down to 25 °C. The H_2 flow (50 mL min^{-1}, 5.0 vol.% H_2 in Ar) was then stabilized and the TPR was performed from 25 °C to 1000 °C (10 °C min^{-1}). H_2 consumption was quantified by a TCD detector.

Oxygen chemisorption was performed in order to determine the number of redox active Mo species on the catalysts. Before the analysis, the samples were activated under 50 mL min^{-1} of pure hydrogen at 300 °C, 5 °C min^{-1} for 1 h. Then, at this same temperature, successive pulses of O_2 were injected until the saturation of the sample. O_2 uptake was quantified by a TCD detector.

The density and nature of acid sites of the catalysts were determined by DRIFTS of adsorbed pyridine using a Nicolet Nexus instrument with a DTGS detector and a quartz cell with CaF_2 windows. The samples were pre-treated at 400 °C under vacuum overnight. Then, the samples were cooled down to 150 °C and a spectrum was recorded in order to use as a reference. At this temperature, pyridine adsorption was carried out for 5 min followed by a purge for 1 h. The spectrum was recorded, and the temperature was further raised to 250, 350 and 450 °C. Adsorption spectra were recorded at a resolution of 2 cm^{-1}, accumulating 64 scans.

3.4. Transformation of FAc

The transformation of 4-(2-furyl)-3-buten-2-one (FAc) in the vapor-phase was carried out in a fixed-bed reactor, operating at an atmospheric pressure of H_2 and 300 °C. The catalysts (pelleted, crushed and sieved to 200–315 μm) were diluted with SiC to avoid localized heating. Prior to the reaction, the catalysts were activated in situ under pure hydrogen (30 mL min^{-1}) at 300 °C for 1 h. The liquid feed, introduced in the reactor by using a kdS scientific syringe, was composed by 4-(2-furyl)-3-buten-2-one as a reactant (3.8% molar), n-heptane (6.0% molar) as an internal standard and ethanol as a solvent. The catalysts were tested at the same W/F value (around 73 g h mol^{-1}). W/F is defined as the catalyst mass (g) divided by the mass flow rate (mol h^{-1}) of the organic feed. The reaction was evaluated during 4.5 h on stream (TOS). The line at the bottom of the reactor was maintained at 5 °C using a circulator Huber mini-chiller. Liquid samples were collected each 30 min and quantified by a Varian 430 chromatograph equipped with a DB-5 capillary column and a flame-ionization detector (FID). Products were identified by an Agilent Technologies 7200/7890A GC-MS, using a HP-5MS capillary column and FID.

The conversion of the FAc and product selectivity were calculated using Equations (1) and (2):

$$X\ (\text{in } \%) = \frac{n^0{}_{FAc} - n_{FAc}}{n^0{}_{FAc}} \times Ac0 \quad (1)$$

$$S_i\ (\text{in mol } \%) = \frac{n_i}{n^0{}_{FAc} - n_{FAc}} \times 100 \quad (2)$$

where $n^0{}_{FAc}$ and n_{FAc} are the number of moles of the reactant FAc (4-(2-furyl)-3-buten-2-one) in the feed and in the collected liquid sample, respectively, and n_i is the number of moles of a given i product.

The total reaction rate (r_{TOT} in mmol g^{-1} h^{-1}) was estimated using Equation (3):

$$r_{TOT}\ (\text{in mmol } g^{-1}\ h^{-1}) = \frac{X.F}{w} \quad (3)$$

where r_{TOT} is the total reaction rate for the FAc transformation, X is the FAc conversion, F is the FAc flow rate (in mmol h^{-1}) and W is catalyst weight (in g).

The thermogravimetric analysis coupled with a mass spectrometer (TGA-MS) was performed in order to verify the formation of the carbonaceous species deposited on the catalysts after the reaction. The measurements were carried out on a SDT Q600 TA Instrument apparatus coupled with a QGA mass spectrometer from Hiden. The analysis was performed up to 1000 °C (heating rate of 10 °C min^{-1}) under air flow (100 mL min^{-1}). The formation of CO_2 was quantified by the mass spectrometer.

4. Conclusions

In this work, molybdenum supported on SBA-15 catalysts was evaluated in the transformation of a furan-based compound (FAc) at 300 °C under atmospheric pressure. The activity of molybdenum oxide as well as the promoter effect of different dopants (Zr, Fe and Al) onto the support was investigated. Molybdenum oxide was active for the hydrogenation of the aliphatic C=C bond and other reactions such as isomerization, condensation and deoxygenation of the carbonyl bond present in the FAc molecule, probably due to its acidity. The addition of Fe as a dopant did not change the activity of the Mo/SBA-15 catalyst, while an improvement in the activity and selectivity to the partially deoxygenated product was observed with the addition of Zr and Al. Mo/Zr-SBA was found to be the most active and selective catalyst into products obtained by cyclisation.

Author Contributions: Conceptualization, C.A.T. and F.R.; methodology, C.A.T. and C.C.; validation, C.A.T. and F.R.; investigation, C.A.T. and C.C.; resources, S.R. and F.R.; data curation, C.A.T.; writing—original draft preparation, C.A.T.; writing—review and editing, F.R.; visualization, F.R.; supervision, F.R.; project administration, F.R.; funding acquisition, F.R. All authors have read and agreed to the published version of the manuscript.

Funding: This research received funding from Coordenacao de Aperfeicoamento de Pessoal de Nivel Superior (CAPES-CAPES-COFECUB program—88881.142911/2017-01) and external financial support from the European Union (ERDF), "Region Nouvelle Aquitaine".

Data Availability Statement: Not applicable.

Acknowledgments: The Chevreul Institute is acknowledged for its help in the development of this work through the ARCHI-CM project supported by the "Ministère de l'Enseignement Supérieur de la Recherche et de l'Innovation", the region "Hauts-de-France" and the ERDF program of the European Union and the "Métropole Européenne de Lille.

Conflicts of Interest: The authors declare no conflict of interest.

References

1. Patel, M.; Kumar, A. Production of Renewable Diesel through the Hydroprocessing of Lignocellulosic Biomass-Derived Bio-Oil: A Review. *Renew. Sustain. Energy Rev.* **2016**, *58*, 1293–1307. [CrossRef]
2. Wong, S.S.; Shu, R.; Zhang, J.; Liu, H.; Yan, N. Downstream Processing of Lignin Derived Feedstock into End Products. *Chem. Soc. Rev.* **2020**, *49*, 5510–5560. [CrossRef] [PubMed]
3. Kroyan, Y.; Wojcieszyk, M.; Kaario, O.; Larmi, M. Modeling the impact of sustainable aviation fuel properties on end-use performance and emissions in aircraft jet engines. *Energy* **2022**, *255*, 124470. [CrossRef]
4. Gutiérrez-Antonio, C.; Gómez-Castro, F.I.; de Lira-Flores, J.A.; Hernández, S. A Review on the Production Processes of Renewable Jet Fuel. *Renew. Sustain. Energy Rev.* **2017**, *79*, 709–729. [CrossRef]
5. Chen, S.; Zhou, G.; Miao, C. Green and Renewable Bio-Diesel Produce from Oil Hydrodeoxygenation: Strategies for Catalyst Development and Mechanism. *Renew. Sustain. Energy Rev.* **2019**, *101*, 568–589. [CrossRef]
6. Huber, G.W.; Chheda, J.N.; Barrett, C.J.; Dumesic, J.A. Production of Liquid Alkanes by Aqueous-Phase Processing of Biomass-Derived Carbohydrates. *Sci. New Ser.* **2005**, *308*, 1446–1450. [CrossRef]
7. West, R.M.; Liu, Z.Y.; Peter, M.; Dumesic, J.A. Liquid Alkanes with Targeted Molecular Weights from Biomass-Derived Carbohydrates. *ChemSusChem* **2008**, *1*, 417–424. [CrossRef]
8. Xing, R.; Subrahmanyam, A.V.; Olcay, H.; Qi, W.; van Walsum, G.P.; Pendse, H.; Huber, G.W. Production of Jet and Diesel Fuel Range Alkanes from Waste Hemicellulose-Derived Aqueous Solutions. *Green Chem.* **2010**, *12*, 1933. [CrossRef]
9. Fakhfakh, N.; Cognet, P.; Cabassud, M.; Lucchese, Y.; de Los Ríos, M.D. Stoichio-Kinetic Modeling and Optimization of Chemical Synthesis: Application to the Aldolic Condensation of Furfural on Acetone. *Chem. Eng. Process.* **2008**, *47*, 349–362. [CrossRef]
10. Hora, L.; Kelbichová, V.; Kikhtyanin, O.; Bortnovskiy, O.; Kubička, D. Aldol Condensation of Furfural and Acetone over MgAl Layered Double Hydroxides and Mixed Oxides. *Catal. Today* **2014**, *223*, 138–147. [CrossRef]

11. Desai, D.S.; Yadav, G.D. Green Synthesis of Furfural Acetone by Solvent-Free Aldol Condensation of Furfural with Acetone over La_2O_3–MgO Mixed Oxide Catalyst. *Ind. Eng. Chem. Res.* **2019**, *58*, 16096–16105. [CrossRef]
12. Xu, M.; Célérier, S.; Comparot, J.-D.; Rousseau, J.; Corbet, M.; Richard, F.; Clacens, J.-M. Upgrading of Furfural to Biofuel Precursors via Aldol Condensation with Acetone over Magnesium Hydroxide Fluorides $MgF_{2-x}(OH)_x$. *Catal. Sci. Technol.* **2019**, *9*, 5793–5802. [CrossRef]
13. Faba, L.; Díaz, E.; Ordóñez, S. Hydrodeoxygenation of Acetone–Furfural Condensation Adducts over Alumina-Supported Noble Metal Catalysts. *App. Catal. B Environm.* **2014**, *160–161*, 436–444. [CrossRef]
14. Faba, L.; Díaz, E.; Ordóñez, S. Role of the Support on the Performance and Stability of Pt-Based Catalysts for Furfural–Acetone Adduct Hydrodeoxygenation. *Catal. Sci. Technol.* **2015**, *5*, 1473–1484. [CrossRef]
15. Ramos, R.; Tišler, Z.; Kikhtyanin, O.; Kubička, D. Towards Understanding the Hydrodeoxygenation Pathways of Furfural–Acetone Aldol Condensation Products over Supported Pt Catalysts. *Catal. Sci. Technol.* **2016**, *6*, 1829–1841. [CrossRef]
16. Xia, Q.-N.; Cuan, Q.; Liu, X.-H.; Gong, X.-Q.; Lu, G.-Z.; Wang, Y.-Q. Pd/$NbOPO_4$ Multifunctional Catalyst for the Direct Production of Liquid Alkanes from Aldol Adducts of Furans. *Angew. Chem.* **2014**, *126*, 9913–9918. [CrossRef]
17. Yang, J.; Li, S.; Zhang, L.; Liu, X.; Wang, J.; Pan, X.; Li, N.; Wang, A.; Cong, Y.; Wang, X.; et al. Hydrodeoxygenation of furans over Pd-FeO_x/SiO_2 catalyst under atmospheric pressure. *App. Catal. B Environ.* **2017**, *201*, 266–277. [CrossRef]
18. Sirous-Rezaei, P.; Jae, J.; Ha, J.-M.; Ko, C.H.; Kim, J.M.; Jeon, J.-K.; Park, Y.-K. Mild hydrodeoxygenation of phenolic lignin model compounds over a $FeReO_x$/ZrO_2 catalyst: Zirconia and rhenium as efficient dehydration promoters. *Green Chem.* **2018**, *20*, 1472–1483. [CrossRef]
19. Shetty, M.; Murugappan, K.; Prasomsri, T.; Green, W.H.; Román-Leshkov, Y. Reactivity and Stability Investigation of Supported Molybdenum Oxide Catalysts for the Hydrodeoxygenation (HDO) of m-Cresol. *J. Catal.* **2015**, *331*, 86–97. [CrossRef]
20. Gonçalves, V.O.O.; Ciotonea, C.; Arrii-Clacens, S.; Guignard, N.; Roudaut, C.; Rousseau, J.; Clacens, J.-M.; Royer, S.; Richard, F. Effect of the Support on the Hydrodeoxygenation of m -Cresol over Molybdenum Oxide Based Catalysts. *App. Catal. B Environm.* **2017**, *214*, 57–66. [CrossRef]
21. Yoon, B.S.; Kim, K.-J.; Cho, E.H.; Park, H.-R.; Roh, H.-S.; Ko, C.H. Enhanced Fe-Cr dispersion on mesoporous silica support using surfactant-assisted melt-infiltration for the water-gas shift reaction in waste-to-hydrogen processes. *Int. J. Hydrogen Energy* **2023**, *48*, 24894–24903. [CrossRef]
22. Wu, S.; Han, Y.; Zou, Y.-C.; Song, J.-W.; Zhao, L.; Di, Y.; Liu, S.-Z.; Xiao, F.-S. Synthesis of heteroatom substituted SBA-15 by the "pH-adjusting" method. *Chem. Mater.* **2004**, *16*, 486–492. [CrossRef]
23. Ungureanu, A.; Dragoi, B.; Hulea, V.; Cacciaguerra, T.; Meloni, D.; Solinas, V.; Dumitriu, E. Effect of aluminium incorporation by the "pH-adjusting" method on the structural, acidic and catalytic properties of mesoporous SBA-15. *Microporous Mesoporous Mater.* **2012**, *163*, 51–64. [CrossRef]
24. Ungureanu, A.; Dragoi, B.; Chirieac, A.; Ciotonea, C.; Royer, S.; Duprez, D.; Mamede, A.S.; Dumitriu, E. Composition-dependent morphostructural properties of Ni-Cu oxide nanoparticles confined within the channels of ordered mesoporous SBA-15 silica. *ACS Appl. Mater. Interfaces* **2013**, *5*, 3010–3025. [CrossRef]
25. Ciotonea, C.; Mazilu, I.; Dragoi, B.; Catrinescu, C.; Dumitriu, E.; Ungureanu, A.; Alamdari, H.; Petit, S.; Royer, S. Confining for stability: Heterogeneous catalysis with transition metal (oxide) nanoparticles confined in the secondary pore network of mesoporous scaffolds. *ChemNanoMat* **2017**, *3*, 233–237. [CrossRef]
26. Sfeir, A.; Teles, C.A.; Marinova, M.; Vezin, H.; Dacquin, J.-P.; Lofberg, A.; Laassiri, S.; Rojer, S. Switching on/off molybdenum nitride catalytic activity in ammonia synthesis through modulating metal-support interaction. *Faraday Discuss.* **2023**, *243*, 126–147. [CrossRef]
27. Regalbuto, J.R.; Ha, J.-W. A corrected procedure and consistent interpretation for temperature programmed reduction of supported MoO_3. *Catal. Lett.* **1994**, *29*, 189–207. [CrossRef]
28. Teles, C.A.; Ciotonea, C.; Gomes, N.; Gonçalves, V.O.O.; Ungureanu, A.; Catrinescu, C.; Marinova, M.; Clacens, J.-C.; Royer, S.; Noronha, F.B.; et al. Hydrodeoxygenation of m-cresol over Pd-Al-SBA-15 catalysts: Effect of Al content on the deoxygenation reaction pathways. *App. Catal. A Gen.* **2022**, *641*, 118686. [CrossRef]
29. Panagiotopoulou, P.; Martin, N.; Vlachos, D.G. Effect of hydrogen donor on liquid phase catalytic transfer hydrogenation of furfural over a Ru/RuO_2/C catalyst. *J. Mol. Catal. A Chem.* **2014**, *392*, 223–228. [CrossRef]
30. Teles, C.A.; Ciotonea, C.; Le Valant, A.; Canaff, C.; Dhainaut, J.; Clacens, J.-M.; Noronha, F.B.; Richard, F.; Royer, S. Optimization of catalyst activity and stability in the m-cresol hydrodeoxygenation through Ni particle size control. *Appl. Catal. B Environ.* **2023**, *338*, 123030. [CrossRef]
31. Li, Y.; Zhang, W.; Zhang, L.; Yang, Q.; Wei, Z.; Feng, Z.; Li, C. Direct synthesis of Al-SBA-15 mesoporous materials via hydrolysis-controlled approach. *J. Phys. Chem.* **2004**, *108*, 9739–9744. [CrossRef]
32. Ramos, R.; Tišler, Z.; Kikhtyanin, O.; Kubička. Solvent effects in hydrodeoxygenation of furfural-acetone aldol condensation products over Pt/TiO_2 catalyst. *App. Catal. A Gen.* **2017**, *530*, 174–183. [CrossRef]
33. Prasomsri, T.; Shetty, M.; Murugappan, K.; Roman-Leshkov, Y. Insights into the catalytic activity and surface modification of MoO_3 during the hydrodeoxygenation of lignin-derived model compounds into aromatic hydrocarbon under low hydrogen pressures. *Energy Environ. Sci.* **2014**, *7*, 2660–2669. [CrossRef]
34. Prasomsri, T.; Nimmanwudipong, T.; Roman-Leshkov, Y. Effective hydrodeoxygenation of biomass-derived oxygenates into unsaturated hydrocarbons by MoO_3 using low H_2 pressures. *Energy Environ. Sci.* **2013**, *6*, 1732–1738. [CrossRef]

35. Valencia, D.; Garcia-Cruz, I.; Ramirez-verduzco, L.F.; Aburto, J. Adsorption of biomass-derived products on MoO_3: Hydrogen bonding interactions under the spotlight. *ACS Omega* **2018**, *3*, 14165–14172. [CrossRef] [PubMed]
36. Farah, B.; Lancelot, C.; Blanchard, P.; Richard, F.; Lamonier, C. Beneficial effect of W incorporation in supported Mo-based catalysts for the HDO of m-cresol. *ChemCatChem* **2023**, *15*, e2022014. [CrossRef]
37. Hashem, A.M.; Adbel-Ghany, A.E.; El-Tawil, R.S.; Indris, S.; Ehrenberg, H.; Mauger, A.; Julien, C.M. Amorphous Mo_5O_{14}-type/carbon nanocomposite with enhanced electrochemical capability for lithium-ion batteries. *Nanomaterials* **2020**, *10*, 8. [CrossRef]